Article

Dynamics of Large Elongated RNA by NMR Carbon Relaxation

Alexandar L. Hansen, and Hashim M. Al-Hashimi

J. Am. Chem. Soc., **2007**, 129 (51), 16072-16082 • DOI: 10.1021/ja0757982

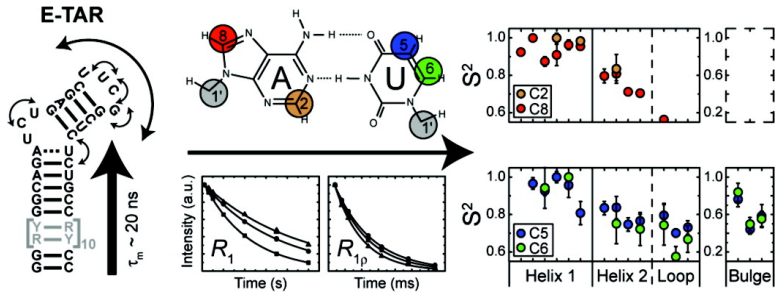

More About This Article

Additional resources and features associated with this article are available within the HTML version:

- Supporting Information
- Links to the 4 articles that cite this article, as of the time of this article download
- Access to high resolution figures
- Links to articles and content related to this article
- Copyright permission to reproduce figures and/or text from this article

View the Full Text HTML

J|A|C|S
ARTICLES
Published on Web 11/30/2007

Dynamics of Large Elongated RNA by NMR Carbon Relaxation

Alexandar L. Hansen and Hashim M. Al-Hashimi*

Department of Chemistry and Biophysics, The University of Michigan, Ann Arbor, Michigan 48109

Received August 2, 2007; E-mail: hashimi@umich.edu

Abstract: We present an NMR strategy for characterizing picosecond-to-nanosecond internal motions in uniformly $^{13}C/^{15}N$-labeled RNAs that combines measurements of R_1, $R_{1\rho}$, and heteronuclear $^{13}C\{^1H\}$ NOEs for protonated base (C2, C5, C6, and C8) and sugar (C1′) carbons with a domain elongation strategy for decoupling internal from overall motions and residual dipolar coupling (RDC) measurements for determining the average RNA global conformation and orientation of the principal axis of the axially symmetric rotational diffusion. TROSY-detected pulse sequences are presented for the accurate measurement of nucleobase carbon R_1 and $R_{1\rho}$ rates in large RNAs. The relaxation data is analyzed using a model free formalism which takes into account the very high anisotropy of overall rotational diffusion ($D_{ratio} \approx 4.7$), asymmetry of the nucleobase CSAs and noncollinearity of C−C, C−H dipolar and CSA interactions under the assumption that all interaction tensors for a given carbon experience identical isotropic internal motions. The approach is demonstrated and validated on an elongated HIV-1 TAR RNA ($\tau_m \approx 18$ ns) both in free form and bound to the ligand argininamide (ARG). Results show that, while ARG binding reduces the amplitude of collective helix motions and local mobility at the binding pocket, it leads to a drastic increase in the local mobility of "spacer" bulge residues linking the two helices which undergo virtually unrestricted internal motions ($S^2 \approx 0.2$) in the ARG bound state. Our results establish the ability to quantitatively study the dynamics of RNAs which are significantly larger and more anisotropic than customarily studied by NMR carbon relaxation.

Introduction

Many regulatory RNAs undergo large conformational transitions that are essential for executing their functions.[1−3] Stepwise changes in RNA conformation induced by sequential protein recognition events allow complex ribonucleoproteins, such as the ribosome and spliceosome, to assemble in a hierarchically ordered manner.[4] Riboswitches control gene expression by undergoing large changes in secondary and tertiary structure in response to recognition of metabolite molecules.[5,6] The global conformation of ribozymes change during their catalytic cycles in order to satisfy the diverse structural requirements associated with substrate binding, catalysis, and product release.[7,8] Although it is clear that many RNA structures must change in a specific manner in order to carry out their functions, the mechanism by which these conformational changes occur is not fully understood. Recent studies suggest that the inherent dynamical properties of RNA structure play an important role in directing these conformational transitions.[9,10]

Nuclear magnetic resonance (NMR) spectroscopy is a powerful technique for characterizing the dynamical properties of biomolecules, uniquely providing site-resolved dynamical information over a broad range (ps−s) of time scales.[10−13] The most commonly used approach to obtaining dynamical information involves analyzing transverse (R_2) and longitudinal (R_1) relaxation rates together with heteronuclear Overhausser enhancements (NOEs) using the model free formalism[14] to obtain information regarding internal fluctuations occurring at subnanosecond time scales. Although this approach is now widely used in NMR studies of protein dynamics using backbone amide nitrogens as relaxation probes, a number of factors continue to complicate applications to nucleic acids. The scarcity of suitable imino nitrogen probes has made it crucial to resort to other relaxation probes, including deuterium[15] or more commonly the protonated carbons.[13,16−22] However, carbon spins pose unique challenges in both measurement and data interpretation due to

(1) Al-Hashimi, H. M. *ChemBioChem* **2005**, *6*, 1506−1519.
(2) Micura, R.; Hobartner, C. *ChemBioChem* **2003**, *4*, 984−990.
(3) Leulliot, N.; Varani, G. *Biochemistry* **2001**, *40*, 7947−7956.
(4) Williamson, J. R. *Nat. Struct. Biol.* **2000**, *7*, 834−837.
(5) Mandal, M.; Breaker, R. R. *Nat. Rev. Mol. Cell Biol.* **2004**, *5*, 451−463.
(6) Schwalbe, H.; Buck, J.; Furtig, B.; Noeske, J.; Wohnert, J. *Angew. Chem., Int. Ed.* **2007**, *46*, 1212−1219.
(7) Lilley, D. M. *Methods Mol. Biol.* **2004**, *252*, 77−108.
(8) Walter, N. G.; Engelke, D. R.; Harris, D. A.; Rueda, D. *Biologist (London)* **2002**, *49*, 199−203.
(9) Furtig, B.; Buck, J.; Manoharan, V.; Bermel, W.; Jaschke, A.; Wenter, P.; Pitsch, S.; Schwalbe, H. *Biopolymers* **2007**, *86*, 360−383.
(10) Getz, M.; Sun, X.; Casiano-Negroni, A.; Zhang, Q.; Al-Hashimi, H. M. *Biopolymers* **2007**, *86*, 384−402.
(11) Palmer, A. G., III; Massi, F. *Chem. Rev.* **2006**, *106*, 1700−1719.
(12) Mittermaier, A.; Kay, L. E. *Science* **2006**, *312*, 224−228.
(13) Shajani, Z.; Varani, G. *Biopolymers* **2007**, *86*, 348−359.
(14) Lipari, G.; Szabo, A. *J. Am. Chem. Soc.* **1982**, *104*, 4546−4559.
(15) Vallurupalli, P.; Kay, L. E. *J. Am. Chem. Soc.* **2005**, *127*, 6893−6901.
(16) Williamson, J. R.; Boxer, S. G. *Nucleic Acids Res.* **1988**, *16*, 1529−1540.
(17) Hall, K. B.; Tang, C. G. *Biochemistry* **1998**, *37*, 9323−9332.
(18) Boisbouvier, J.; Wu, Z.; Ono, A.; Kainosho, M.; Bax, A. *J. Biomol. NMR* **2003**, *27*, 133−142.
(19) Duchardt, E.; Schwalbe, H. *J. Biomol. NMR* **2005**, *32*, 295−308.
(20) Shajani, Z.; Varani, G. *J. Mol. Biol.* **2005**, *349*, 699−715.
(21) Ravindranathan, S.; Kim, C. H.; Bodenhausen, G. *J. Biomol. NMR* **2005**, *33*, 163−174.

10.1021/ja0757982 CCC: $37.00

presence of C−C interactions and sizable asymmetric chemical shift anisotropy (CSA) tensors. Perhaps an even greater problem that has surfaced only more recently is that globally flexible RNAs can violate the "decoupling approximation" which is invoked in the model free formalism which assumes that internal and overall motions are not correlated to one another.[14] This violation occurs because helices can move collectively at time scales approaching that of overall molecular tumbling (τ_m). These motions can also lead to substantial deformations in RNA, resulting in spatially coupled changes in overall reorientation.[23−28] Such motional couplings can add an intractable layer of complexity to the analysis of relaxation data.

Recently, we reported a domain-elongation strategy for decoupling internal motions in RNA from overall diffusion as a prerequisite for quantitatively interpreting relaxation data.[25] Here, a terminal RNA helix is elongated using a stretch of 22 NMR-invisible Watson−Crick base-pairs in an otherwise uniformly $^{13}C/^{15}N$-labeled RNA. In addition to decoupling collective movements of helices from overall reorientation, elongation reduces the overall tumbling rate, thus broadening the timescale sensitivity of the relaxation data. Measurement of imino nitrogen relaxation data in elongated RNAs (E-RNA) has allowed resolution of collective helix motions in a variety of structural contexts that otherwise evade detection in non-elongated RNA owing to couplings with overall reorientation.[23,25,26] So far, the limited number of available imino nitrogen probes have not allowed for a comprehensive site-specific characterization of dynamics, particularly in the functionally important nonhelical regions. Nevertheless, qualitative analysis of resonance intensities suggests the presence of near τ_m local motions that also evade detection in non-elongated RNAs.[23−26]

There have been significant advances in applying carbon relaxation in studies of dynamics in relatively small nucleic acids that tumble nearly isotropically ($D_{ratio} < 2.0$).[13,19,20,27,29] The CSA tensors for the protonated carbons[30−32] have also recently been determined in solution using residual CSA (RCSA) and spin relaxation measurements thus resolving a great source of uncertainty in dynamical interpretation of the relaxation data. However, the need to decouple internal from overall motions via domain-elongation results in a significant increase in molecular weight and anisotropy of the RNA which in turn introduces a number of new challenges. First, the increase in the carbon transverse relaxation rates can make accurate measurement of relaxation data difficult. Second, homonuclear carbon relaxation contributions increase dramatically[18,22,33] and can no longer be ignored. Third, the significant increase in structural anisotropy of E-RNA renders relaxation data strongly dependent on the orientation of the noncollinear C−H, C−C and asymmetric CSA interactions relative to the principal axis (D_{zz}) of overall rotational diffusion.

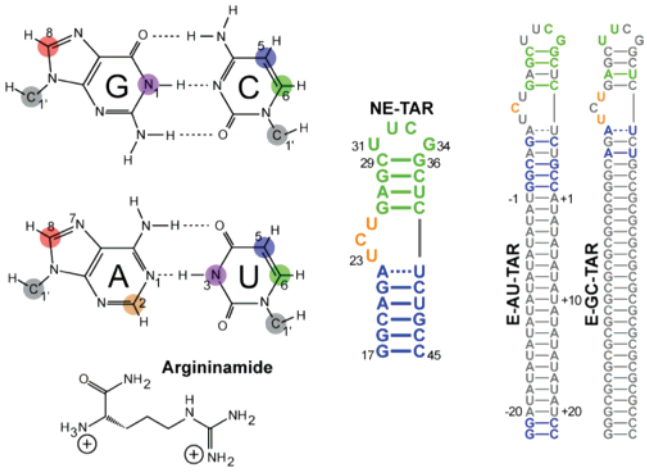

Figure 1. Carbon relaxation probes and elongation of HIV-1 TAR. Shown are the base and sugar carbon relaxation probes, secondary structure of non-elongated (NE-TAR) and elongated (E-GC-TAR and E-AU-TAR) TAR and chemical structure of argininamide. Uniformly $^{13}C/^{15}N$-labeled and unlabeled RNA residues are shown in color and in gray, respectively.

Here, we describe application of carbon relaxation in characterizing the dynamics of large, highly anisotropic, uniformly $^{13}C/^{15}N$-labeled RNA with specific application to elongated HIV-1 TAR (E-TAR)[34−36] both in free form and bound to argininamide, a ligand mimic of the TAR cognate protein target Tat (Figure 1). Our results provide fundamental new insights into the internal motions in TAR and their role in adaptive recognition as well as establish the ability to quantitatively study the dynamics of RNAs significantly larger and more anisotropic than customarily studied by NMR carbon relaxation.

Materials and Methods

NMR Spectroscopy. All NMR samples were prepared by in vitro transcription as described previously.[25] The NMR buffer consisted of 15 mM sodium phosphate, 0.1 mM EDTA, and 25 mM NaCl at pH ≈ 6.4. The argininamide-bound TAR sample also contained ~8 mM argininamide (Sigma-Aldrich). All NMR experiments were performed at 298 K, unless specified otherwise, using an Avance Bruker 600 MHz spectrometer equipped with a 5 mm triple-resonance cryogenic probe. NMR spectra were processed using nmrPipe[37] and analyzed using NMRView.[38]

Longitudinal (R_1) and rotating-frame ($R_{1\rho}$) relaxation rates were measured for nucleobase carbons C2, C5, C6 and C8 (Figure 1) using a TROSY detected (TD) experiment shown in Figure 2a.[39−41] A non-TROSY version of the pulse sequence was used to measure relaxation data for C1′. Setup and acquisition parameters are listed in Tables S1

(22) Johnson, J. E., Jr.; Julien, K. R.; Hoogstraten, C. G. *J. Biomol. NMR* **2006**, *35*, 261−274.
(23) Sun, X.; Zhang, Q.; Al-Hashimi, H. M. *Nucleic Acids Res.* **2007**, *35*, 1698−1713.
(24) Shajani, Z.; Drobny, G.; Varani, G. *Biochemistry* **2007**, *46*, 5875−5883.
(25) Zhang, Q.; Sun, X.; Watt, E. D.; Al-Hashimi, H. M. *Science* **2006**, *311*, 653−656.
(26) Getz, M. M.; Andrews, A. J.; Fierke, C. A.; Al-Hashimi, H. M. *RNA* **2006**, 251−266.
(27) Showalter, S. A.; Hall, K. B. *Methods Enzymol.* **2005**, *394*, 465−480.
(28) Zhang, Q.; Throolin, R.; Pitt, S. W.; Serganov, A.; Al-Hashimi, H. M. *J. Am. Chem. Soc.* **2003**, *125*, 10530−10531.
(29) Showalter, S. A.; Baker, N. A.; Tang, C. G.; Hall, K. *J. Biomol. NMR* **2005**, *32*, 179−193.
(30) Bryce, D. L.; Grishaev, A.; Bax, A. *J. Am. Chem. Soc.* **2005**, *127*, 7387−7396.
(31) Hansen, A. L.; Al-Hashimi, H. M. *J. Magn. Reson.* **2006**, *179*, 299−307.
(32) Ying, J.; Grishaev, A.; Bryce, D. L.; Bax, A. *J. Am. Chem. Soc.* **2006**, *128*, 11443−11454.
(33) Boisbouvier, J.; Brutscher, B.; Simorre, J. P.; Marion, D. *J. Biomol. NMR* **1999**, *14*, 241−252.
(34) Puglisi, J. D.; Tan, R.; Calnan, B. J.; Frankel, A. D.; Williamson, J. R. *Science* **1992**, *257*, 76−80.
(35) Aboul-ela, F.; Karn, J.; Varani, G. *Nucleic Acids Res.* **1996**, *24*, 3974−3981.
(36) Bannwarth, S.; Gatignol, A. *Curr. HIV Res.* **2005**, *3*, 61−71.
(37) Delaglio, F.; Grzesiek, S.; Vuister, G. W.; Zhu, G.; Pfeifer, J.; Bax, A. *J. Biomol. NMR* **1995**, *6*, 277−293.
(38) Johnson, B. A.; Blevins, R. A. *J. Biomol. NMR* **1994**, *4*, 603−614.
(39) Igumenova, T. I.; Palmer, A. G., III. *J. Am. Chem. Soc.* **2006**, *128*, 8110−8111.
(40) Zhu, G.; Xia, Y.; Nicholson, L. K.; Sze, K. H. *J. Magn. Reson.* **2000**, *143*, 423−426.
(41) Loria, J. P.; Rance, M.; Palmer, A. G. *J. Biomol. NMR* **1999**, *15*, 151−155.

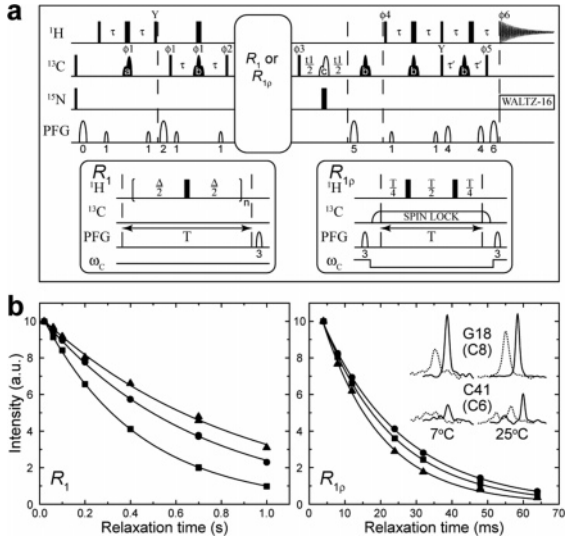

Figure 2. TROSY-detected (TD) experiments for the measurement of nucleobase carbon R_1 and $R_{1\rho}$ in uniformly $^{13}C/^{15}N$-labeled RNA. (a) TD pulse sequence. Narrow and wide rectangles indicate 90° and 180° pulses, respectively. Selective pulses *a* and *b* are on resonance, and *c* is off resonance. The *a* pulse selectively inverts carbon magnetization of interest. The *b* (*c*) pulses selectively refocus (invert) carbon magnetization to eliminate C−C scalar coupling evolution. $\tau = 1/4J_{CH}$ and $\tau' = \tau - 1/2G_6$. Pulse field gradients (PFG) are sine shaped with the following amplitude (G/cm)/durations (ms): $G_0 = -6.0/1.0$, $G_1 = 0.5/0.25$, $G_2 = 8.0/1.0$, $G_3(R_1) = 3.3/1.0$, $G_3(R_{1\rho}) = 6.0/1.0$, $G_4 = 5.0/0.15$, $G_5 = 9.0/0.6$, $G_6 = 9.052/0.15$. Phases are for Bruker spectrometers. Unless noted otherwise, all pulses have an *x* phase. The phase cycle is $\phi_1 = 4(x, -x)$, $\phi_2 = 4(y)\ 4(-y)$, $\phi_3 = 2(y, y, -y, -y)$, $\phi_4 = -y$, $\phi_5 = -x$, and $\phi_6 = (x, -x, -x, x, -x, x, x, -x)$. Axial peaks are shifted to the edge of the spectrum by incrementing ϕ_3 and ϕ_6 by 180° for each t_1 increment. ω_C represents the carrier offset frequency. In the R_1 element, Δ is set to 10 ms, and the carrier remains on resonance, while in the $R_{1\rho}$ element the carrier is shifted before and after the adiabatic passages. Detailed experimental parameters are provided in Tables S1 and S2. (b) Representative R_1 and $R_{1\rho}$ decays for residues in the elongated helix I (triangles), helix II (circles), and the bulge (squares). (Inset) Representative slices along the indirect carbon dimension comparing the TROSY (solid line) and non-TROSY (dotted line) detected experiments. Intensities are normalized relative to the TROSY G18 peak at each temperature.

and S2. High power off-resonance spinlocks were used in the $R_{1\rho}$ experiment to minimize contributions from chemical exchange while suppressing Hartman-Hahn type transfers to scalar coupled carbon spins (vide infra, Table S1). Accurate alignment of the $\pm C_z$ magnetization to and from the effective field tilt angle θ at the beginning and end of the relaxation period was achieved using adiabatic half passages.[42] Spin lock powers were carefully calibrated as previously described (Figure S1).[43] The $R_{1\rho}$ rates were corrected for off-resonance effects according to $R_{1\rho} = R_1 \cos^2\theta + R_2 \sin^2\theta$, in which $\theta = \arctan(\nu_{SL}/\Omega)$ is the effective tilt angle of the spinlock field, ν_{SL} is the spinlock field strength in Hz, and Ω is the resonance offset from the spinlock carrier frequency in Hz. All relaxation series were recorded in an interleaved manner with alternating short and long relaxation (T) delays (Table S2). Relaxation rates and errors were determined by fitting intensities to a monoexponential decay using Origin 7.0 (OriginLab Corporation) and in-house software. The $^{13}C\{^1H\}$ NOEs were measured for C2 and C8 using conventional experiments from the intensity ratio with and without proton saturation. NOEs were not measured for C1′, C5, and C6 because the effects of homonuclear C−C relaxation lead to significant errors in the measurements.[44] The measured relaxation data are listed in Tables S3−S5.

Model Free Analysis. The carbon relaxation data was combined and analyzed with the nitrogen data reported by Zhang et al.[25] using an extended model free approach[14,45] implemented with in-house software that incorporates spectral density functions[46] (eqs 4−5) that can account for asymmetric CSAs under axially symmetric overall diffusion and includes contributions from all, noncollinear C−C and C−H dipolar interactions. In these calculations, it was assumed that the principal axes of all interaction tensors (i.e., CSA, C−H, and C−C dipole) experience identical isotropic internal motions. All relaxation data were calculated using eqs 1−6 and analyzed separately for E-GC-TAR and E-AU-TAR.

Motionally averaged bond lengths of 1.104,[32] 1.041,[47] and 1.115 Å[30,47] were used for the nucleobase C−H, imino N−H, and sugar C1′−H1′ bonds, respectively. The solution NMR-derived CSAs were used for C2, C5, C6, and C8[32] and C1′.[30] The static DFT-computed imino nitrogen CSAs[48] were used after uniform scaling by a factor of 0.913[47] to account for the similar motional averaging of the CSA and N−H dipolar interaction.[49] The orientation of D_{zz} with respect to helices I and II was assumed to be equal to the orientation of the principal direction of alignment (S_{zz}) in Pf1 phage[50,51] determined by order tensor analysis[52,53] of RDCs measured in E-TAR.[54] Several studies have shown that in the absence of electrostatic attraction, the orientation of the alignment tensor frame is similar to that of the diffusion tensor.[55−57] Virtually identical D_{zz} and S_{zz} orientations (deviations ~3°) are also predicted for E-TAR based on its structure using HydroNMR[58] and PALES,[59] respectively. The experimentally derived S_{zz} orientation deviates from perfect coincidence with the elongated helix axis by ~6°. The hydrodynamically predicted[58] D_{ratio} value of 4.7 was assumed[25] noting that ±10% variations had a negligible impact on the analysis (data not shown). For globally rigid E-TAR+ARG, the hydrodynamically predicted D_{ratio} (4.7) and D_{zz} orientation obtained for the RDC-derived NE-TAR+ARG interhelical conformation[60] was assumed as previously described.[25] The local structure of the bulge was modeled into the RDC-derived interhelical conformation using previous NOE structures of TAR (1ANR for free TAR[35] and both 1ARJ[61] and 1AJU[62] for ARG bound TAR).

The global correlation time, τ_m, was initially determined through a χ^2 minimization of the elongated helix C2, C8, and N1/3 relaxation data (for which NOE data was also available) while also allowing a single internal correlation time (τ_e) and order parameter (S^2) to vary. The latter was crucial for determining a global correlation time that agrees with all carbon and nitrogen relaxation data. Analysis of the carbon data while excluding nitrogen data resulted in nearly identical motional parameters (S^2 rmsd < 0.02). The τ_m values obtained for free

(42) Mulder, F. A. A.; de Graaf, R. A.; Kaptein, R.; Boelens, R. *J. Magn. Reson.* **1998**, *131*, 351−357.
(43) Palmer, A. G., III; Kroenke, C. D.; Loria, J. P. *Methods Enzymol.* **2001**, *339*, 204−238.
(44) Yamazaki, T.; Muhandiram, R.; Kay, L. E. *J. Am. Chem. Soc.* **1994**, *116*, 8266−8278.
(45) Clore, G. M.; Szabo, A.; Bax, A.; Kay, L. E.; Driscoll, P. C.; Gronenborn, A. M. *J. Am. Chem. Soc.* **1990**, *112*, 4989−4991.
(46) Spiess, H. W. *NMR: Basic Princ. Prog.* **1978**, *15*, 55−214.
(47) Case, D. A. *J. Biomol. NMR* **1999**, *15*, 95−102.
(48) Czernek, J. *J. Phys. Chem. A* **2001**, *105*, 1357−1365.
(49) Hallock, K. J.; Lee, D. K.; Ramamoorthy, A. *J. Chem. Phys.* **2000**, *113*, 11187−11193.
(50) Hansen, M. R.; Mueller, L.; Pardi, A. *Nat. Struct. Biol.* **1998**, *5*, 1065−1074.
(51) Clore, G. M.; Starich, M. R.; Gronenborn, A. M. *J. Am. Chem. Soc.* **1998**, *120*, 10571−10572.
(52) Saupe, A. *Angew. Chem., Int. Ed. Engl.* **1968**, *7*, 97−112.
(53) Musselman, C.; Pitt, S. W.; Gulati, K.; Foster, L. L.; Andricioaei, I.; Al-Hashimi, H. M. *J. Biomol. NMR* **2006**, *36*, 235−249.
(54) Zhang, Q.; Stelzer, A.; Fisher, C. K.; Al-Hashimi, H. M. *Nature* **2007**. Manuscript in press.
(55) Tjandra, N.; Bax, A. *Science* **1997**, *278*, 1111−1114.
(56) Bax, A.; Tjandra, N. *J. Biomol. NMR* **1997**, *10*, 289−292.
(57) van Dijk, A. D. J.; Fushman, D.; Bonvin, A. *Proteins: Struct., Funct., Bioinf.* **2005**, *60*, 367−381.
(58) Garcia de la Torre, J.; Huertas, M. L.; Carrasco, B. *J. Magn. Reson.* **2000**, *147*, 138−146.
(59) Zweckstetter, M.; Bax, A. *J. Am. Chem. Soc.* **2000**, *122*, 3791−3792.
(60) Pitt, S. W.; Majumdar, A.; Serganov, A.; Patel, D. J.; Al-Hashimi, H. M. *J. Mol. Biol.* **2004**, *338*, 7−16.
(61) Aboul-ela, F.; Karn, J.; Varani, G. *J. Mol. Biol.* **1995**, *253*, 313−332.
(62) Brodsky, A. S.; Williamson, J. R. *J. Mol. Biol.* **1997**, *267*, 624−639.

(16.8−18.1 ± 0.8 ns) and ARG bound TAR (17.6−18.6 ± 1.4 ns) were in good agreement with values reported previously by ^{15}N relaxation (18.9−19.0 ± 0.9 and 18.4−18.6 ± 0.6 ns, respectively).[25] Following determination of the global correlation time, internal motional parameters were selected from five possible single-field models (see Results and Discussion).[63] Only models 1−3 were tested for the C1′, C5, and C6 data since NOEs could not be measured reliably. The internal motional parameters, $S^2_{f/s}$ and τ_e, were minimized using a simplex algorithm[64] following a grid search with initial step sizes set sufficiently small to avoid trapping the simplex algorithm into false minima. For models including internal correlation times, the results were inspected for model elimination before being subjected to model selection.[65] The best internal motional parameters were selected using the Akaike's Information Criteria (AIC).[66]

The error in the internal motional parameters due to uncertainty in experimental measurements was obtained by performing Monte Carlo simulations of each R_1, R_2, and NOE set while leaving the global diffusion parameters fixed. In each simulation the relaxation data was perturbed randomly based on measurement error and minimized assuming the same error as the original data set. Motional parameter uncertainties were then determined from the trimmed mean of the distribution of 1000 model free parameters, including removal of simulations falling under model elimination criteria.[65] To estimate the uncertainty in motional parameters arising from potential errors in the assumed CSAs, the model free analysis was repeated using the solid-state NMR CSAs for all spins,[67] and the errors were generously estimated as the difference between the two sets of computed motional parameters. Likewise, conservative errors due to potential variations in the D_{zz} orientation were estimated by repeating the model free analysis assuming D_{zz} is perfectly co-incident with the elongated helix axis and taking the difference between the two sets of motional parameters. For bulge residues, the standard deviation of the parameters determined using all input conformations was computed. The final error in the derived motional parameters was calculated as the root sum square of the individual error contributions. All motional parameters and uncertainties are listed in Tables S6 and S7.

Results and Discussion

Contributions to Carbon Relaxation. It is instructive to consider the various relaxation contributions to our targeted carbons. The longitudinal and transverse carbon relaxation rates, taking into account all homo- and heteronuclear interactions, can be best understood through examination of their time dependencies:[18,44]

$$\frac{d(\Delta C_z(t))}{dt} = -(\rho_{C,CSA} + \sum_i \rho_{CH_i} + \sum_j \rho_{CC_j}{}^0 + \sum_k \rho_{CC_k}{}^1)(\Delta C_z(t)) - \sum_i \sigma_{CH_i}(\Delta H_{i,z}(t)) - \sum_j \sigma_{CC_j}{}^0(\Delta C_{j,z}(t)) - \sum_k \sigma_{CC_k}{}^1(\Delta C_{k,z}(t)) \quad (1)$$

$$\frac{d(\Delta C_+(t))}{dt} = -(R_{2,CSA} + \sum_i R_{2,CH_i} + \sum_j R_{2,CC_j}{}^0 + \sum_k R_{2,CC_k}{}^1)(\Delta C_+(t)) + R_{ex} \quad (2)$$

in which the various auto- (ρ) and cross- (σ) relaxation longitudinal rates and R_2 transverse relaxation rates are given by:

$$\rho_{CX} = R_{1,CX} = \frac{1}{10} D_{CX}{}^2\{6g_2^{DD}(\omega_C + \omega_X) + g_2^{DD}(\omega_C - \omega_X) + 3g_2^{DD}(\omega_C)\}$$

$$\sigma_{CX} = \frac{1}{10} D_{CX}{}^2\{6g_2^{DD}(\omega_C + \omega_X) - g_2^{DD}(\omega_C - \omega_X)\}$$

$$R_{2,CX} = \frac{1}{20} D_{CX}{}^2\{6g_2^{DD}(\omega_C + \omega_X) + 6g_2^{DD}(\omega_X) + g_2^{DD}(\omega_C - \omega_X) + 3g_2^{DD}(\omega_C) + 4g_2^{DD}(0)\}$$

$$\rho_{CSA} = R_{1,CSA} = \frac{1}{10} C_C{}^2\{3g_2^{CSA}(\omega_C)\}$$

$$R_{2,CSA} = \frac{1}{20} C_C{}^2\{3g_2^{CSA}(\omega_C) + 4g_2^{CSA}(0)\} \quad (3)$$

D_{CX} and C_C are the familiar dipolar coupling ($\mu_0 h\gamma_C\gamma_X/8\pi^2 r_{CX}^3$) and CSA ($\omega_C\ \sigma_{zz}$) constants, R_{ex} is the chemical exchange contribution to transverse relaxation, and g_2 is the half-sided Fourier transform of the autocorrelation function describing the time dependence of the CSA (g_2^{CSA}) or dipolar (g_2^{DD}) interactions due to internal motions.[46] In the absence of asymmetric relaxation mechanisms, g_2 is equal to the common spectral density function, $J(\omega)$. R_2, ρ, and σ subscripts indicate the type of relaxation mechanism (e.g., C−C dipolar, C−H dipolar, or CSA) while superscripts of homonuclear carbon dipolar interactions indicate the number of protons bound to the neighboring carbon (e.g., $\rho_{C5C4} = \rho_{CC}^0$). The carbon−carbon cross-relaxation in eq 1 is separated into two terms because the magnetization state of neighboring carbons after the INEPT, and thus the contribution to the initial decay rate from cross-relaxation, will vary depending on whether the carbon is attached to a proton or not.

For an RNA with $\tau_m > 15$ ns, the dipolar contribution to R_2 from neighboring nitrogens, protons (>2 Å), and carbons (>1.3 Å) are negligible (<2%), and can be safely ignored. Both the R_1 and R_2 for purine C2 and C8 and the R_2 for C5 and C6 are dominated by C−H dipolar and carbon CSA relaxation. The CSA contribution to R_2 ranges between 25 and 45% at 600 MHz, but can be as large as 35−65% at 900 MHz. For R_1, the corresponding CSA contribution at 600/900 MHz is 15−30%/24−33% for C2 and C8 and 5−30%/10−40% for C5 and C6. The CSA contribution to R_1 and R_2 for C1′ is negligible (<4% even at 900 MHz) and R_2 is dominated by C−H dipolar relaxation. In contrast, the C−C dipolar contribution from nearby carbons to R_1 for C5 (40−80%), C6 (20−70%), and C1′ (15−60%) is significant. As shown in eq 3, of the three mechanisms in question, only CC dipolar contains a $g_2(0)$ term arising from $g_2(\omega_x - \omega_y)$ difference term. This term increases linearly as a function of correlation time, whereas all other spectral density terms decrease dramatically. The C−C auto- and cross-relaxation will therefore require careful consideration for the latter carbons. Longitudinal and transverse CSA_C/DD_{CC}, DD_{CC}/DD_{CC}, DD_{CC}/DD_{CH}, and DD_{C5H5}/DD_{C5H6} or DD_{C6H6}/DD_{C6H5} cross-correlated relaxation can be safely ignored as they are typically 2 to 3 orders of magnitude smaller than the auto relaxation rates. The CSA_C/DD_{CH} cross-correlated relaxation and C−H cross-relaxation contributions to R_1 and CSA_C/DD_{CH}

(63) Mandel, A. M.; Akke, M.; Palmer, A. G. *J. Mol. Biol.* **1995**, *246*, 144−163.
(64) Nelder, J. A.; Mead, R. *Comput. J.* **1965**, *7*, 308−313.
(65) d'Auvergne, E. J.; Gooley, P. R. *J. Biomol. NMR* **2006**, *35*, 117−135.
(66) d'Auvergne, E. J.; Gooley, P. R. *J. Biomol. NMR* **2003**, *25*, 25−39.
(67) Stueber, D.; Grant, D. M. *J. Am. Chem. Soc.* **2002**, *124*, 10539−10551.

cross-correlated relaxation contribution to R_2, which can be on the order of the relaxation measurement itself, must be suppressed using an appropriate proton decoupling scheme during the relaxation period.[68,69] For the $R_{1\rho}$ scheme of Figure 2a we use a decoupling scheme of Massi et al.[68,69] which uses a pair of 180 pulses at T/4 and 3T/4 and performs well over a wide range of spinlock field strengths.

TROSY-Detected Pulse Sequences for the Measurement of Nucleobase Carbon R_1 and $R_{1\rho}$. We implemented pulse sequences (Figure 2a) for measuring carbon relaxation that address two problems encountered in applications to large RNAs. The greater transverse relaxation rate for carbon spins (3−6 times greater than for nitrogen) leads to unfavorable loss in sensitivity that can make accurate measurement of relaxation data difficult. We used TROSY[70] detection (TD) to improve sensitivity and resolution in the R_1 and $R_{1\rho}$ experiment for the nucleobase carbons C2, C5, C6, and C8, all of which have sizable CSAs that give rise to favorable TROSY effects.[33,71] Following the normal relaxation period of longitudinal or in-phase ^{13}C magnetization, TROSY coherence selection in both ^{13}C and ^{1}H dimensions is used for detection of the slowly relaxing component resulting from destructive interference between CSA and dipole−dipole (DD) interactions. In addition, selective carbon pulses are used throughout to eliminate signal losses to neighboring scalar coupled carbons ($J_{C5C6} \approx 67$ Hz, $J_{C1'C2'} \approx 40$ Hz) during the INEPT transfers and indirect detection period. The TD experiments yielded sensitivity improvements on the order of 50%, 65%, and 40% for C2, C6, and C8, respectively (Figure 2b, inset) for E-TAR at 600 MHz with $\tau_m = 18$ ns, in agreement with theoretical predictions.[71] The TD experiments allowed us to reliably measure relaxation data for E-TAR at 280 K with $\tau_m \approx 35$ ns corresponding to a ∼150 nt RNA at 298 K, that could not otherwise be measured using conventional sequences due to overlap and/or poor signal-to-noise ratio.

The second problem encountered is that C−C dipolar interactions increase dramatically with molecular weight and large cross-relaxation rates can lead to multiexponential behavior when measuring R_1 for C5, C6, and C1′.[44] Although the C−C cross-relaxation rate is approximately equal and opposite in magnitude to C−C auto-relaxation (eqs 1 and 3), their mutual cancellation[18,44] only occurs if the equilibrium magnetization of the neighboring carbons is identical to that of the carbon of interest and the relaxation time delays do not significantly exceed $1/R_1$. In our R_1 experiment, cross-relaxation to neighboring carbons is suppressed as originally described by Kay and co-workers by gradient dephasing carbon magnetization at the beginning of the pulse sequence followed by selective excitation of the carbon nucleus of interest using a selective inversion ^{13}C 180° pulse during the first INEPT period.[44] This is particularly important for C5, C6, and C1′ in which neighboring carbons can contribute significantly to R_1 (eq 1). The remaining C−C dipolar auto-relaxation contribution is then explicitly taken into account in the model free analysis of the relaxation data. Other features implemented in the pulse sequences include the use of selective off-resonance spinlocks in the $R_{1\rho}$ experiment that minimize Hartman−Hahn transfers to scalar coupled carbon spins, such as between C5−C6, C1′−C2′, and C4/6−C8 to <0.1% maximum transfer efficiency. This was accomplished by ensuring that the difference in the effective field strengths experienced by two coupled carbon spins (C_x and C_y) is much greater than $^nJ_{xy}$ (Table S1).[19,44,72] The effects of CSA_C/DD_{CH} cross-correlated relaxation and C−H cross-relaxation are also suppressed by proton decoupling during the relaxation period.[68,69]

Figure 2b shows representative R_1 and $R_{1\rho}$ fits obtained using the TD experiment. Monoexponential behavior was observed in all cases, indicating the absence of any detectable C−C cross-relaxation and Hartman−Hahn transfer. Excellent agreement was also observed between the R_1 and $R_{1\rho}$ rates measured using the TD and conventional experiment although the latter had ∼24% and 82% greater fitting errors for R_1 and $R_{1\rho}$, respectively (data not shown). Having confirmed the monoexponential behavior of the TD relaxation experiments for all spins in E-TAR, an optimized sampling strategy was adopted for the remaining experiments (see Supporting Information)[73,74]

Analysis of R_2/R_1 Values. In Figure 3, we compare the carbon R_2/R_1 values measured in non-elongated TAR (NE-TAR) (Figure 3a), E-TAR (3b), and E-TAR bound to ARG (3c). Different R_2/R_1 values are observed for the various carbon types, reflecting their inherently different relaxation mechanisms and, in particular, differences in R_1 due to differing numbers of C−C interactions. In NE-TAR, similar R_2/R_1 values were observed for the two helical domains. Normally, this would be interpreted as evidence that the RNA reorients as a rigid unit and that the two helices are therefore held rigid relative to one another. However, given the similar size of the two helices, one cannot rule out that they may reorient semi-independently of one another. These motions could go undetected because either they cause similar reductions in the R_2/R_1 values observed in both helices or they occur at time scales slower than overall tumbling. Fortunately, domain elongation resolves this ambiguity. Unlike NE-TAR, the R_2/R_1 values measured in the short helix of E-TAR are attenuated relative to counterparts measured in the elongated helix (Figure 3b). This uniform attenuation is observed across a variety of carbons, which have C−H, C−C, and CSA interaction tensors spanning diverse orientations in different residues. This suggests that the short helix moves collectively and semi-independently relative to the elongated helix at time scales faster than the overall tumbling of E-TAR. This underscores the ease by which collective helix motions can easily go undetected in small nonelongated RNA such as NE-TAR. The addition of ARG to E-TAR leads to an increase in virtually all of the short helix R_2/R_1 values, including residues at the apical loop that are remote from the bulge ARG binding site, such that they are now far more similar to values measured in the elongated helix. This is exactly as would be expected if ARG were to arrest the collective helix motions in agreement with previous RDC studies.[60,54]

(68) Korzhnev, D. M.; Skrynnikov, N. R.; Millet, O.; Torchia, D. A.; Kay, L. E. *J. Am. Chem. Soc.* **2002**, *124*, 10743−10753.
(69) Massi, F.; Johnson, E.; Wang, C.; Rance, M.; Palmer, A. G., III. *J. Am. Chem. Soc.* **2004**, *126*, 2247−2256.
(70) Pervushin, K.; Riek, R.; Wider, G.; Wuthrich, K. *Proc. Natl. Acad. Sci. U.S.A.* **1997**, *94*, 12366−12371.
(71) Brutscher, B.; Boisbouvier, J.; Pardi, A.; Marion, D.; Simorre, J. P. *J. Am. Chem. Soc.* **1998**, *120*, 11845−11851.
(72) Bax, A.; Davis, D. G. *J. Magn. Reson.* **1985**, *63*, 207−213.
(73) Jones, J. A. *J. Magn. Reson.* **1997**, *126*, 283−286.
(74) Jones, J. A.; Hodgkinson, P.; Barker, A. L.; Hore, P. J. *J. Magn. Reson. B* **1996**, *113*, 25−34.

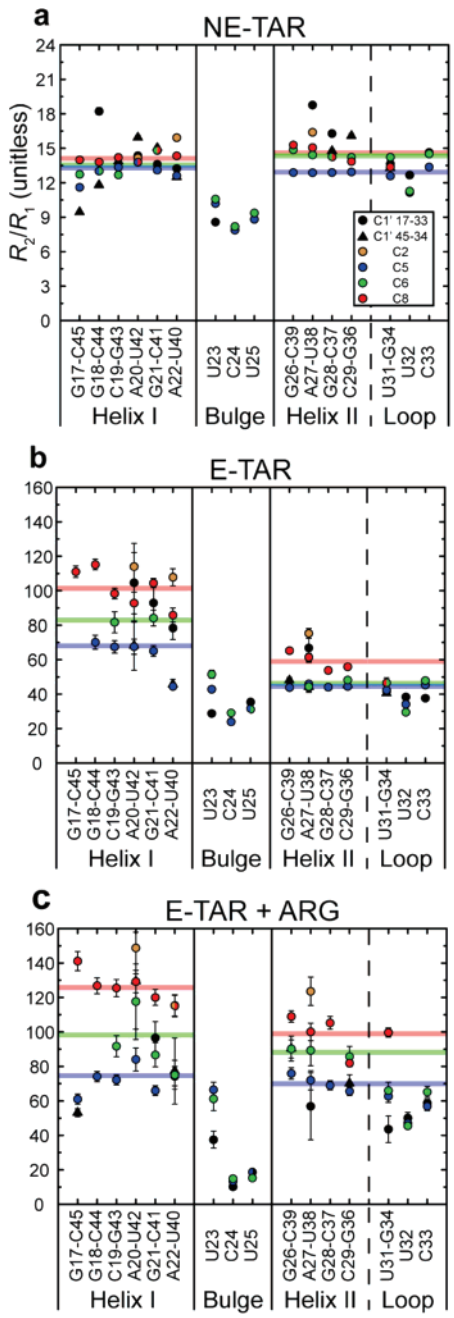

Figure 3. Carbon R_2/R_1 values for (a) free non-elongated TAR (NE-TAR), (b) free elongated TAR (E-TAR), and (c) elongated TAR in complex with ARG (E-TAR + ARG). Values for C1′, C2, C5, C6, and C8 values are indicated in black, brown, blue, green, and red, respectively. Horizontal lines in blue, green, and red indicate the average R_2/R_1 value in a given helix for C5, C6, and C8, respectively.

For both free NE-TAR and E-TAR, significantly attenuated R_2/R_1 values were observed for bulge residues, particularly the "spacer" residues C24 and U25, indicating that the interhelix linker is highly flexible. However, the relative degree of attenuation is much greater for E-TAR, likely reflecting greater sensitivity to internal motions owing to its much slower overall molecular tumbling rate. An extreme example is that the E-TAR R_2/R_1 values appear to expose local mobility at the helix I A22-U40 base-pair that is not observed in NE-TAR. The addition of ARG does not significantly affect bulge residue U23, leads to apparent stabilization of the A22-U40 base-pair, and causes a dramatic reduction in R_2/R_1 and therefore an apparent increase

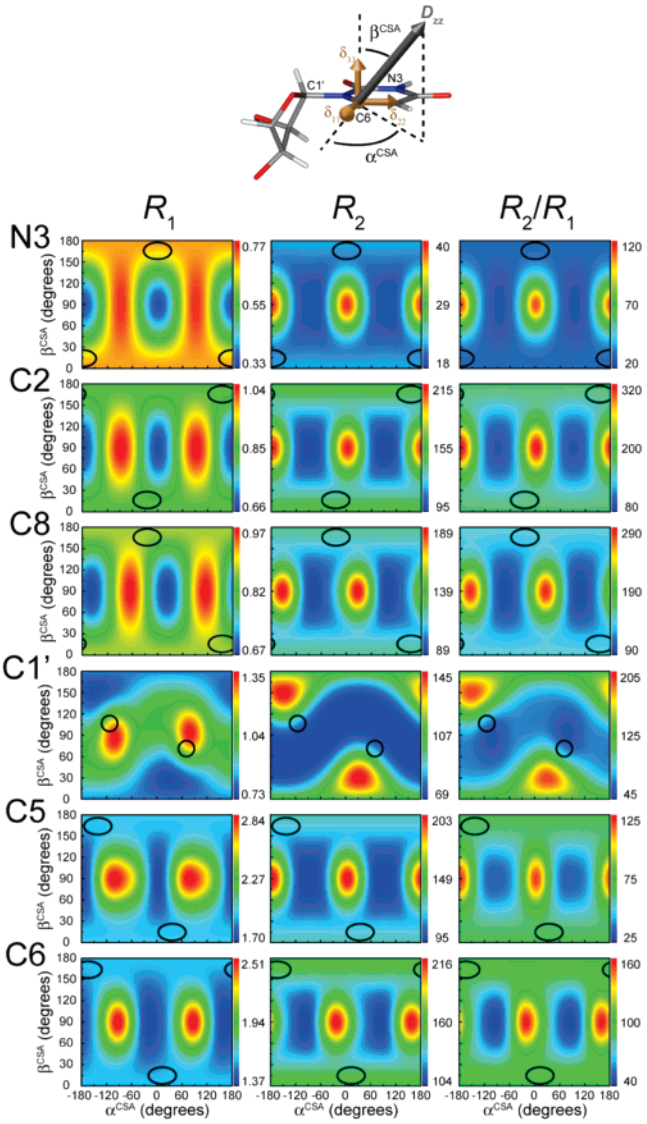

Figure 4. Orientational dependence of relaxation data in elongated RNA. Shown are the computed R_1, R_2, and R_2/R_1 values for imino nitrogen (N3) and carbons (C2 C5 C6 C8 C1′) as a function of the orientation of the principal axis of diffusion (D_{zz}) relative to the principal axis system of the CSA tensor for each spin as defined by the polar angles α^{CSA} and β^{CSA}. The span of values is depicted to the right of each graph and range from the minimum (blue) to maximum (red) value attainable under the simulation conditions. The expected orientations for spins in the elongated RNA helix assuming D_{zz} is perfectly along the elongated helix axis are highlighted. Calculations assumed $\tau_m = 18.5$ ns, $D_{ratio} = 4.7$, $S_t^2 = 0.9$, and $\tau_{eff} = 100$ ps.

in the local mobility of bulge residues C24 and U25, some of which have R_2/R_1 values approaching those observed in NE-TAR.

Orientational Dependence of Carbon Relaxation Data. Unlike the nearly isotropically tumbling NE-TAR ($D_{ratio} \approx 2.0$), spin relaxation in E-TAR ($D_{ratio} \approx 4.7$) strongly depends on the orientation of the principal axis (D_{zz}) of the axially symmetric rotational diffusion tensor relative to the relevant dipolar and CSA interaction tensors. Since the relative orientation of the C−H, C−C, and carbon CSA tensors can be assumed to be known, this orientational dependence can be specified on the basis of the angles α^{CSA} and β^{CSA} that orient D_{zz} relative to the principal axis system (PAS) of the CSA tensor (Figure 4). This orientational dependence, together with the noncollinearity

of C−C, C−H, and CSA interactions, makes the nucleobase carbon R_2/R_1 a complex function of average orientation and internal and global motional parameters which cannot be interpreted as easily as R_2/R_1 values obtained for the case of an axially symmetric CSA that is collinear with a single dominant dipolar interaction, as is normally assumed for amide and imino nitrogens.[75]

It has generally been assumed that the imino nitrogen CSAs are axially symmetric with principal direction (δ_{11}) oriented along the N−H dipolar vector. In this case, relaxation only depends on the angle between the N−H bond and D_{zz}. However, both solid-state NMR[67] and DFT studies[76] suggest that, like nucleobase carbons, the imino nitrogen CSAs, especially those in hydrogen-bonded Watson−Crick base-pairs, are asymmetric and deviate from coincidence with the N−H dipolar vector (∼20−30°). This modifies the orientational dependence of nitrogen relaxation by only a modest amount, given that the CSA contribution remains small at 600 MHz. Nevertheless, this leads to observation of minimum and maximum R_2 and R_1 values, respectively, for orientations in which D_{zz} is perpendicular not only to the N−H bond vector but also to both the δ_{11} and δ_{33} principal axes of the CSA tensor ($\beta \approx 90°$ and $\alpha \approx 90°$) (Figure 4). The CSA orientational contributions are more pronounced for the nucleobase carbons due to their larger CSAs, and in the cases of C1′, C5, and C6, the orientational dependence of R_1 is further modified by dependence on the orientation of C−C bonds (Figure 4). For C1′, the orientational dependence is principally governed by the orientation of the C−H bond relative to D_{zz}, which is also non-co-incident with the principal axes of the CSA tensor (Figure 4).

For imino nitrogens, the R_2/R_1 values measured in the elongated helix in which D_{zz} is assumed to be perfectly along the long axis of the E-RNA represent approximate lower-bound values expected for a globally rigid structure. Only marginally smaller R_2/R_1 values (<10% of the range of R_2/R_1) can be observed for orientations that maintain the N−H dipolar vector and both δ_{11} and δ_{33} perpendicular to D_{zz}. Thus, the observation of R_2/R_1 values that are substantially lower than those measured in the elongated helix can, to a good approximation, be interpreted as evidence for internal motions. The more complicated orientational dependence of the carbon R_2 and R_2/R_1 is such that the values observed in the elongated helices do not correspond to perfect minima. Hence, the observation of attenuated R_2 and R_2/R_1 in regions outside the elongated helices cannot as easily be interpreted as evidence for internal motions since a similar degree of attenuation can arise from unique static orientations. This underscores the importance of taking into account the orientational dependence of various relaxation contributions in the dynamical interpretation of the relaxation data.

Model Free Analysis. The carbon and nitrogen relaxation data was analyzed using a model free analysis that takes into account noncollinearity of relevant spin interactions and their distinct orientational dependencies. In principle, separate motional parameters need to be specified for each CSA, C−H, and C−C relaxation mechanism, as the interaction tensors are all non-coincident to one another. As a first approximation, we assume that the interaction tensors experience identical isotropic internal motions. A recent molecular dynamics simulation of TAR revealed similar motional amplitudes for the nucleobase C−H and N−H bonds in a given residue.[51] With this assumption, a single set of motional parameters is needed to describe the internal motional amplitudes (S) and correlation times (τ). The spectral density function $g_2(\omega)$ by Spiess[46] can be used to take into account the asymmetry of the CSA under highly anisotropic diffusion. By expanding the function according to the extended model free formalism,[45] and including contributions from C−C and C−H dipolar interactions, one can interpret the relaxation data in terms of up to two distinct internal motional modes:[32,46,77]

$$g_2^{\lambda}(\omega) = \sum_{i=0}^{2} c_i^{\lambda}\left(\frac{S_f^2 S_s^2 \tau_i}{1+\omega^2\tau_i^2} + \frac{(1-S_f^2)\tau_{i,f}}{1+\omega^2\tau_{i,f}^2} + \frac{(S_f^2 - S_f^2 S_s^2)\tau_{i,s}}{1+\omega^2\tau_{i,s}^2}\right) \quad (4)$$

where S_f^2 and S_s^2 are order parameters describing the amplitudes of the fast and slow internal motions and τ_F and τ_S describe their internal correlation times, respectively. $\tau_{i,n}^{-1} = \tau_i^{-1} + \tau_n^{-1}$ ($i = 0, 1, 2$ and $n =$ f or s), in which $\tau_0^{-1} = 6\,D_S - 2\,D_a$, $\tau_1^{-1} = 6\,D_S - D_a$ and $\tau_2^{-1} = 6\,D_S + 2\,D_a$ with $D_a = D_{zz} - 1/2\,(D_{xx} + D_{yy})$, $D_S = 1/3\,(D_{xx} + D_{yy} + D_{zz})$, and $\tau_m = (6\,D_S)^{-1}$. For axially symmetric overall diffusion, the coefficients c_i^{λ} are given by:

$$c_0^{\lambda} = \left(\frac{3\cos^2\beta^{\lambda} - 1}{2} - \frac{\eta^{\lambda}}{2}\cos(2\alpha^{\lambda})\sin^2\beta^{\lambda}\right)^2$$

$$c_1^{\lambda} = \frac{1}{3}\left[\left(\frac{\eta^{\lambda}}{2}\cos(2\alpha^{\lambda})\sin(2\beta^{\lambda}) + 3\cos\beta^{\lambda}\sin\beta^{\lambda}\right)^2 + (\eta^{\lambda}\sin(2\alpha^{\lambda})\sin\beta^{\lambda})^2\right]$$

$$c_2^{\lambda} = \frac{1}{3}\left[\left(\frac{\eta^{\lambda}}{4}\cos(2\alpha^{\lambda})(3+\cos(2\beta^{\lambda})) - \frac{3}{2}\sin^2\beta^{\lambda}\right)^2 + (\eta^{\lambda}\sin(2\alpha^{\lambda})\cos\beta^{\lambda})^2\right] \quad (5)$$

in which η^{λ} is the asymmetry of the interaction (λ = CSA or DD) with $\eta_{CSA} = (\sigma_{xx} - \sigma_{yy})/\sigma_{zz} \leq 1$, and $\eta_{DD} = 0$. The angles α^{λ} and β^{λ} are the polar angles defining the orientation of the principal axis of diffusion (D_{zz}) relative to the axially symmetric dipolar ($\alpha^{DD} = 0$ and β^{DD}) and asymmetric CSA (α^{CSA} and β^{CSA}) interaction frame. Note that DD includes both C−H and C−C vectors, each of which has unique orientations relative to D_{zz}. Equation 4 has four unknown local parameters (S_f^2, S_s^2, τ_f, τ_s) whereas only 2 (3) measurements have been made for C1′, C5, and C6 (^{15}N, C2, and C8) nuclei. For this reason, the five standard single field models have been used in this study[63] and selected using Akaike's Information Criteria (AIC, see Materials and Methods).[66]

Model 1 → $S_s^2 = 1$, $S_f^2 = S_t^2$, $\tau_f = \tau_s = 0$, $R_{ex} = 0$

Model 2 → $S_s^2 = 1$, $S_f^2 = S_t^2$, $\tau_s = 0$, $R_{ex} = 0$

Model 3 → $S_s^2 = 1$, $S_f^2 = S_t^2$, $\tau_f = \tau_s = 0$

Model 4 → $S_s^2 = 1$, $S_f^2 = S_t^2$, $\tau_s = 0$

Model 5 → $\tau_f = 0$, $R_{ex} = 0$

(75) Tjandra, N.; Feller, S. E.; Pastor, R. W.; Bax, A. *J. Am. Chem. Soc.* **1995**, *117*, 12562−12566.
(76) Czernek, J.; Fiala, R.; Sklenar, V. *J. Magn. Reson.* **2000**, *145*, 142−146.
(77) Chang, S. L.; Tjandra, N. *J. Magn. Reson.* **2005**, *174*, 43−53.

Deriving dynamical parameters from the relaxation data using eqs 1−5 is greatly facilitated by having a priori knowledge regarding the average orientation of spin interaction tensors (α^λ and β^λ) relative to D_{zz}. Although elongation is expected to align D_{zz} nearly perfectly along the elongated helix axis, deciphering the orientation of D_{zz} relative to other fragments such as helix II can be challenging, particularly for the globally flexible free E-TAR. In our study, we used the average orientation of the two helices as obtained from an order tensor analysis of RDCs recently measured in E-TAR[54] using Pf1 phage[50,51] as an ordering medium. The orientation of D_{zz} was assumed to be either equal to the RDC-derived principal orientation of alignment (S_{zz}) or perfectly along the elongated helix axis (similar results were obtained in the two cases). For the globally rigid and more well-defined TAR+ARG complex, the previous RDC-derived interhelical orientation was assumed along with a hydrodynamically predicted D_{zz} orientation, as previously described.[25] The local structure of the bulge was modeled using previous NOE structures of TAR (1ANR for free TAR[35] and both 1ARJ[61] and 1AJU[62] for ARG bound TAR). In all cases, the overall diffusion tensor was assumed to be axially symmetric with a hydrodynamically computed D_{ratio} value of 4.7 ± 10%.

The inherently large uncertainty for the C1′, C5, and C6 NOEs due to C−C interactions[44] made it impossible to assess the validity of model 5 during the model selection for those spins. However, model 5 was selected consistently for the more isolated C2 and C8 carbons in helix II, for which more reliable NOE measurements were available, supporting the existence of at least two motional modes in helix II. Some carbons in helix I also resulted in selection of model 5. However, the total amplitude of motions ($S_f^2 \times S_s^2$) for these carbons remained comparable in magnitude to the corresponding S_f^2 value obtained for carbons in helix I with models 1−3. For simplicity, we chose to report the total order parameter $S_t^2 = S_f^2$ (models 1−4) or $S_f^2 \times S_s^2$ (model 5) which, unlike the internal correlation time, is primarily dependent on $g_2(0)$ terms which can be accurately defined by the R_2 and R_1 rates. The much greater uncertainty in the internal correlation times (Tables S6,7) precluded their quantitative interpretation. However, any observable collective motions must occur at rates faster than overall diffusion.

The impact of using solution versus solid-state CSAs[67] was also explored. For the majority of carbons (C1′, C5, and C8), this had a small impact on the derived motional parameters (rmsd between two S_t^2 sets <0.037), which is on the order of the variations expected due to measurement uncertainty (on average <0.039). Larger differences were observed for C6 (rmsd ≈ 0.074), for which the largest difference exists between the solution and solid-state CSAs. The C6 S_t^2 values obtained using the solution NMR CSAs were systematically smaller than all other carbons, including C5 on the same nucleobase in both free and ARG bound TAR. Assuming that C5 and C6 in a given base should have similar motional parameters, the best agreement is observed when using the solution CSAs for C5[32] and solid-state CSAs for C6.[67] It is noteworthy that the C6 CSAs were also the least reliably determined in the RCSA solution NMR study.[32] The main results shown in Figure 5 are therefore based on solution NMR CSAs for C1′, C2, C5, and C8 and the solid-state NMR CSA for cytosine C6, which is assumed to be the same for uridine and cytosine. Finally, we note that small

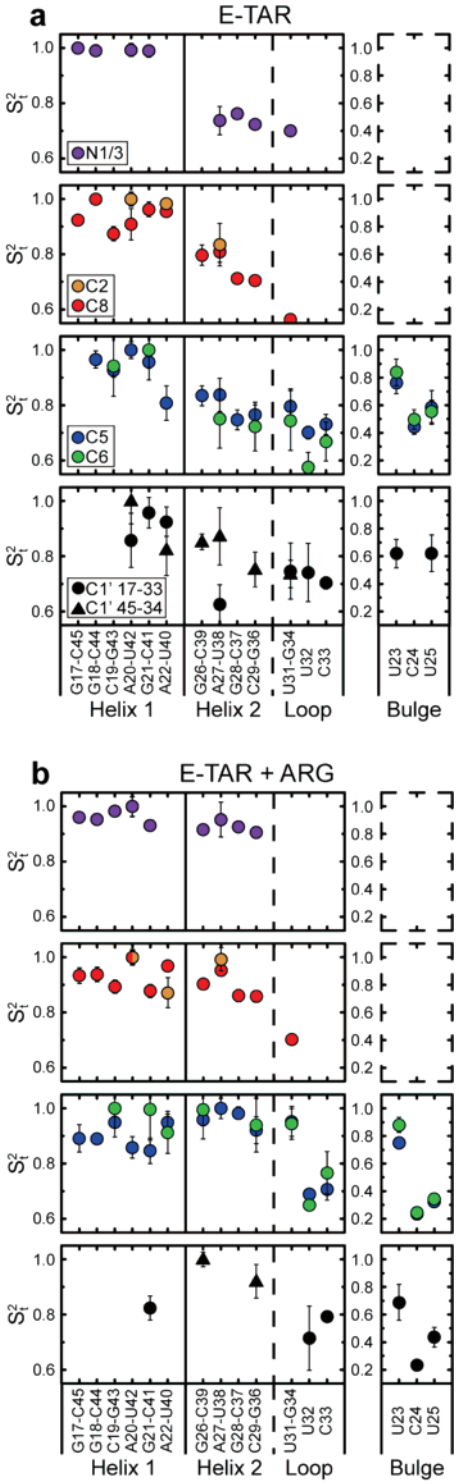

Figure 5. Amplitude of internal motions in free and ARG bound TAR. The total spin relaxation order parameter $S_t^2 = S_f^2 \times S_s^2$ is shown for (a) free E-TAR and (b) E-TAR + ARG. The S_t^2 values are normalized for a given carbon type (C1′ C2 C5 C6 C8) and for nitrogen (N1 and N3) to have the maximum allowed value of 1. Conservative error bars account for uncertainty in the measurement, CSA, and D_{zz} orientation (see Materials and Methods).

differences in the absolute magnitude of S_t^2 were observed for various carbon types (Tables S6 and S7). While this could reflect real differences in the dynamics experienced by different carbons, for example due to anisotropic motions, it may also be the result of small discrepancies in calibrating the motionally

averaged bond lengths and CSAs from carbon to carbon. In order to make comparisons between spin types, the S_t^2 values have been normalized such that the highest value (lowest amplitude) for each nucleus is equal to 1.0.

The normalized carbon S_t^2 values in free and ARG bound TAR are shown in Figure 5. Conservative error bars are shown to account for uncertainty in the measurement, D_{zz} orientation (~6°), and CSAs (see Materials and Methods). The motional parameters obtained for the imino nitrogen relaxation data when conducting the analysis, assuming asymmetric CSAs that are noncollinear with the N−H dipolar vector, are in excellent agreement with those reported previously when assuming axially symmetric CSAs that are collinear with the N−H dipolar vector.[25] This is not surprising, given that CSA contribution to nitrogen relaxation is relatively small at 600 MHz (15%). In addition, the nitrogen motional parameters changed very little when analyzed with or without carbon relaxation data in free and ARG-bound E-TAR (S_t^2 rmsd < 0.02), indicating that the two sets of data are mutually consistent with one another. Despite the large C6 uncertainty, similar S_t^2 values are observed for C5 and C6 in a given nucleobase. Likewise, similar S_t^2 values are observed for carbon and nitrogen spins on the same uridine or guanine nucleobase. This lends support to our assumption that the different interaction tensors experience similar internal motions.

Internal Motions in Free and ARG-Bound E-TAR. With the exception of U40 at the junction of the two helices, limited local mobility is observed in the elongated helix ($S_t^2 \approx 0.9 - 1.0$) in both free (Figure 5a) and ARG-bound (Figure 5b) E-TAR. The high local mobility observed for both the base (C5) and sugar (C1′) in U40 helps explain why its imino proton is exchange broadened out of detection and why it does not form the predicted Watson−Crick hydrogen bond alignment with A22.[60] In contrast, the greater rigidity observed for the nucleobase of A22 is in agreement with the NMR structure of free TAR which shows A22 stacking between U23 and G21.[35] Importantly, the mobility at U40 is arrested upon ARG binding which is consistent with formation of the A22-U40 Watson−Crick hydrogen bond alignment upon ARG recognition.[60]

In free E-TAR, the S_t^2 values observed for the shorter helix II are consistently smaller than counterparts in the elongated helix (Figure 5a). Similar levels of attenuation (~0.75−0.85) are observed for the various carbon and nitrogen spins in the locally stable Watson−Crick base pairs, consistent with a single collective dynamical process that reorients helix II relative to helix I. Although less reliably determined by the relaxation data, the time constant for the slow collective process as obtained by C8 for which NOEs were available (0.8 ± 0.6 ns) is in reasonable agreement with those obtained by nitrogen relaxation (1.4 ± 0.1 ns) and support that the collective motions are diffusion-limited fluctuations that occur at time scales approaching the predicted overall correlation time for the short helix II.[25] Even smaller S_t^2 values are observed for the apical loop residues U32 and C33, which have been shown previously by carbon[19] and deuterium[15] relaxation to be the most locally flexible residues in the UUCG loop. These residues likely experience a combination of collective and local motions. ARG binding leads to the arrest of collective helix motions, as indicated by an increase in the S_t^2 value of virtually every residue in the short helix, including residues at the tip of the helix in the apical loop which show no chemical shift perturbations upon ARG binding. The ARG-induced arrest of collective motions, which has previously also been independently reported by RDCs,[60] exposes local mobility at residues U32 and C33 in the apical loop as a persistent attenuation in S_t^2.

The carbon relaxation data allowed us to quantitatively characterize internal motions in bulge residues for which no suitable imino nitrogen probes are available. For free E-TAR, restricted mobility was observed for the nucleobase of the highly conserved U23 residues, which is critical for Tat recognition, and is in good agreement with NMR structures of free TAR which show that U23 stacks on A22 (Figure 5a).[61] In contrast, very high mobility ($S_t^2 \approx 0.4-0.6$) was observed for the sugar backbone of U23 C1′, which likely facilitates collective motions between the two helices, as well as the nucleobases of C24 and U25, which are only involved in partial stacking interactions (Figure 5a).[61] The limited mobility at U23 is not greatly affected by ARG binding (Figure 5b), consistent with the replacement of stacking interactions with a U23-A27-U38 base-triple alignment in the ARG bound state.[34] In contrast, a dramatic increase in the local mobility of residues C24 and U25 is observed, indicating that they essentially undergo spatially unrestricted motions in the ARG bound state ($S_t^2 \approx 0.2$, Figure 5b). To the best of our knowledge, the S_t^2 values observed for these residues are the smallest reported to date in nucleic acids. The large motional amplitudes observed at C24 and U25 is consistent with their looped out geometry in the TAR+ARG complex in which they are not involved in any interactions.[34,35] These results show that complex formation need not solely be accompanied by conformational stabilization. Rather, mobility in the form of collective helix motions is conserved as local motions in the linker while the interhelix orientation is stabilized in the E-TAR+ARG complex.

Two factors can complicate interpretation of relaxation data in the bulge. First, the carbon CSAs may significantly deviate from values in A-form helices. It is well-known that changes in the chemical environment and hydrogen bonding can lead to changes in all five elements of the CSA tensor.[48,78,79] However, virtually identical S_t^2 values were obtained when using the mononucleotide CSAs obtained by solid-state NMR,[67] even for C6 for which the CSAs are quite different. Second, an average conformation can be difficult to define for these highly flexible residues. However, repeating the analysis using different input bulge conformations from as many as 40 NMR models (see Materials and Methods) also had a negligible impact on the derived S_t^2 values. Thus, the high degree of internal mobility at these sites renders analysis of relaxation data far less sensitive to the details of the CSA and average structure. This suggests that carbon relaxation will provide insights into the dynamics of extremely flexible regions in RNA with high tolerance to potential deviations in the CSAs or lack of knowledge regarding average conformation.

Role of Internal Motions in TAR Adaptation. We previously provided evidence based on qualitative analysis of

(78) Hall, J. B.; Fushman, D. *J. Am. Chem. Soc.* **2006**, *128*, 7855−7870.
(79) Poon, A.; Birn, J.; Ramamoorthy, A. *J. Phys. Chem. B* **2004**, *108*, 16577−16585.

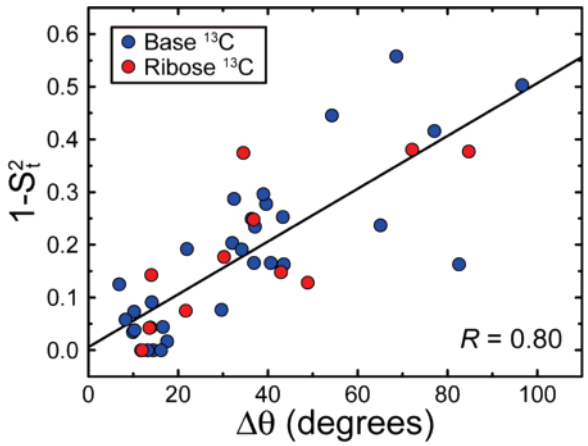

Figure 6. Role of internal motions in TAR adaptation. Shown is a correlated plot between $1 - S_t^2$ and the mean angular difference ($\Delta\theta$) in the orientation of individual sugar (red) and nucleobase (blue) C−H bonds in seven distinct ligand-bound structures of TAR obtained following superposition of helix I as described previously.[25]

resonance intensities in E-TAR that the extent of internal motions at various sites in TAR correlates with the degree to which a given site changes conformation in response to recognition of seven distinct small molecule and ligand targets.[25] Specifically, we observed a correlation ($R = 0.8$) between the normalized intensity observed for a given C−H site in 2D HSQC spectra of E-TAR and the mean angular deviation of the C−H bond ($\Delta\theta$) obtained following superposition of the reference helix I. The latter provides a qualitative measure of the conformational freedom available to a given bond when adapting conformation to bind different targets. With the determination of quantitative order parameters for various sites, we were able to revisit this correlation devoid of the complications that enter analysis of resonance intensities in terms of dynamics, including chemical exchange and the strong orientational dependence of relaxation. As shown in Figure 6, a plot of $\Delta\theta$ versus the $1 - S^2$ reveals a correlation with a similar R factor of 0.80. Thus, sites that undergo the largest changes in conformation upon ligand recognition also undergo the largest-amplitude internal motions in the free state at rates faster than overall diffusion. This provides supporting evidence that intrinsic internal dynamics in TAR play a role in how its conformation adapts upon binding to distinct molecular targets.

Conclusions

By decoupling internal motions from overall reorientation, domain elongation provides the basis for quantitatively characterizing picosecond−nanosecond internal motions in RNA by NMR relaxation methods. Elongation does, however, accentuate potentially unfavorable effects in carbon relaxation studies that grow with molecular weight and structural anisotropy, including the magnitude of C−C relaxation contributions, orientational dependence of relaxation data due to multiple dipolar interactions and highly asymmetric CSAs. Our study suggests that the latter problems can be overcome by combined use of appropriate pulse sequences, analytical methods, and by taking advantage of structural and diffusion tensor orientation information from the measurement of RDCs.

Of particular importance in studies of E-RNA is to have accurate information regarding the asymmetric nucleobase carbon CSAs, including their orientation, which can normally be ignored in isotropically tumbling systems. In this regard, our study benefited tremendously from recent advances in using RCSAs to measure CSAs under solution conditions[30−32] which, when combined with previously reported solid-state NMR values,[67] provide a basis for exploring the potential error arising from CSA uncertainty. Our results suggest that, with the exception of C6, the errors in motional amplitudes for our targeted carbons due to potential variations in CSA are only slightly higher than the error contribution from typical measurement uncertainty. This error contribution becomes smaller with increasing mobility, making analysis of relaxation data highly tolerant to potentially large CSA variations in flexible nonhelical regions.

A potentially much larger source of uncertainty in the analysis of the carbon relaxation data is the orientation of the D_{zz} relative to the RNA structure. Relative to the ideal nitrogen spins, the determination of the overall diffusion tensor parameters by the carbon relaxation data is made more difficult by the more complex dependence of R_2/R_1 on orientational and motional parameters. Clearly, the measurement of additional relaxation data, including at different magnetic fields, can help define the complex, model free parameter space. In our study, we took advantage of RDCs both in defining an average RNA conformation over sub-millisecond time scales and in defining the average orientation of D_{zz} relative to helices I and II.[54] In the latter, we assumed that the principal axis of alignment (S_{zz}) in phage-ordering media is identical to D_{zz}, which seems to be a reasonable assumption given that both properties are primarily governed by the overall molecular shape of the elongated RNA. For highly flexible regions such as bulge residues C24 and U25, the model free analysis is considerably less sensitive to the orientation of D_{zz}.

Our study of TAR confirmed the presence of complex heterogeneous dynamics consisting of local and collective motions that were previously inferred based on a smaller number of imino nitrogen relaxation data and qualitative analysis of motional narrowing of resonances.[25] It also revealed that the internal motions can undergo complex reorganization upon ligand recognition involving a combination of stabilization and, surprisingly, dramatic increases in local mobility. Both the local and collective motions in TAR occur at rates that approach or are slower than the overall molecular tumbling of non-elongated RNAs, and suggest a spectrum of local and collective motions exists at nanosecond-to-microsecond time scales. By expanding the types of relaxation data that are measured, it may be possible to define the time scale and anisotropy of motions as well as long-range aspects of RNA structure.

Acknowledgment. We thank Qi Zhang for the E-AU22-TAR RNA sample, Dr. Erik R. P. Zuiderweg for stimulating discussions, and Dr. Alex Kurochkin for his expertise and for maintenance of the NMR instruments. We gratefully acknowledge the Michigan Economic Development Cooperation and the Michigan Technology Tri-Corridor for the support of the purchase 600 MHz spectrometer. This work was supported by funding from NSF-CAREER (MCB 0644278).

Supporting Information Available: Description of optimized sampling strategy, supporting figure showing spinlock calibration, and six tables summarizing experimental NMR parameters, the measured carbon relaxation data, and model free parameters. This material is available free of charge via the Internet at http://pubs.acs.org.

JA0757982